PERGAMON

Journal of Structural Geology 25 (2003) 1973–1979

JOURNAL OF STRUCTURAL GEOLOGY

www.elsevier.com/locate/jsg

Estimating local strain due to comminution in experimental cataclastic textures

Jafar Hadizadeh[a,*], Walter K. Johnson[b]

[a]*Department of Geography and Geosciences, University of Louisville, Louisville, KY 40292, USA*
[b]*Department of Geological Sciences, University of Kentucky, KY 40506, USA*

Accepted 23 January 2003

Abstract

Cataclastic textures were produced by deforming porous quartz sandstone samples at room temperature, 15–200 MPa confining pressure, and 13–57% strain ($\gamma \sim 2$–20). Particle size distribution (PSD) and fractal dimension (D) values were measured on different digital images of each sample. Over the range of applied axial strain the detectable effects of comminution (particle-size reduction through fracture) on PSD were limited to the population of particles ≥ 7 μm. Textural variable ψ, named comminution intensity, is defined in terms of total sectional area of particle population greater than a critical size S_c. For the Massillon sandstone the S_c is close to four times the suggested value for quartz grinding limit. The comminution intensity vs. axial strain data due to the entire range of applied pressure and strain fits a power function of the form $\epsilon_{11} = \psi^n$, with $0.25 \leq m \leq 0.5$. The local strain due to constrained comminution is then predictable by model function $\epsilon_L = \psi^n$, where $n = 1/m$, with empirical $n = 2.97$ for the studied sandstone. The model predicts relatively monotonous textures for very small and very large strains, while the highest variety of particle size occurs at between 2 and 13% strain. Applications of the method include millimeter to meter scale mapping of the relative degree of comminution in natural fault gouge and the local strain values in experimental samples.

Keywords: Local strain; Cataclastic textures; Porous quartz sandstone

1. Introduction

Numerous studies and models indicate that cataclastic textures in fault gouge contain information about key processes in creep and seismic behavior of faults, including shear localization (e.g. Marone and Scholz, 1989; Mair et al., 2000; Lin, 2001), time-dependent strength of gouge (e.g. Dieterich, 1981; Logan and Rauenzahn, 1987; Biegel et al., 1989; Beeler et al., 1996; Mair and Marone, 1999), evolution of porosity and permeability in fault zones (e.g. Scholz and Anders, 1994; Evans and Chester, 1995; Evans et al., 1997; Zhang et al., 1999; Rawling et al., 2001). However, coupling between microstructural and mechanical analysis of rocks in the brittle regime is weak because of the inherent randomness and discontinuity in cataclastic textures.

A significant proportion of the strain in cataclastic deformation is accommodated by the process named constrained comminution (Sammis et al., 1987) that is particle fragmentation under the effects of a confining pressure. The process results in changing the shape and size of mineral grains, and adjustments in interparticle void spaces. The resulting textures are often characterized by particle size, or particle size distribution (PSD) (e.g. Blenkinsop, 1991; An and Sammis, 1994; Ozkan and Ortoleva, 2000;Blenkinsop and Fernandez, 2000). It has been shown that natural and experimental fault gouge textures exhibit self-similarity (e.g. Sammis et al., 1986, 1987; Marone and Scholz, 1989; Blenkinsop and Fernandez, 2000). The property is characterized by fractal dimension (D), the value of which is readily determined from PSD of the texture. Sammis et al. (1987) suggested that in a gouge with fractal PSD the total strain is correlated with D, and strain per fracture event. Earlier studies have qualitatively characterized deformation intensity in fault gouge based on a clast/matrix ratio (e.g. Sibson, 1977). The size ratio approach is mainly based on the general, but consistent,

* Corresponding author. Tel.: +1-502-852-2691; fax: +1-502-852-4560.
E-mail address: hadizadeh@louisville.edu (J. Hadizadeh).

0191-8141/03/$ - see front matter © 2003 Elsevier Ltd. All rights reserved.
doi:10.1016/S0191-8141(03)00016-6

observation that in constrained comminution particle size decreases with increased strain. While D values have been used to characterize deformation through the state of PSD (e.g. Morgan and Boettcher, 1999; Blenkinsop and Fernandes, 2000), this study is an attempt to find a quantitative expression of strain due to comminution using an analysis of particle size reduction with strain. The study describes a method developed based on textures of experimentally deformed porous quartz sandstone. Measurements are carried out using digital image techniques.

2. Experiments and experimental results

Massilon sandstone is a well-sorted quartz sandstone from south central Ohio, USA with total porosity of 10.47% (mercury porisometer measurements), average grain-size of 33 μm, and typical composition of 92% quartz, 6% opaque, 1.5% clay minerals. We discuss data related to room temperature triaxial compression experiments on 23 air-dry, and four water-saturated cylindrical specimens with a largest rectangular section of 13 × 26 mm. The experiments were carried out in a Heard-type liquid medium machine at confining pressures of 15–200 MPa and axial strain ranging from 13 to 57% at 3×10^{-5}/s strain rate. Here, we will refer to 13–20% as low-strain, 20–40% as medium strain, and 40–57% as high-strain. Shear strain γ corresponding to the applied axial strain could be estimated by $\gamma = \Delta l/\cos\theta d$, where Δl is the actual sample shortening, θ is the average angle between sample fault zone and σ_1 direction, and d is the average fault zone thickness. Based on our observations, we assumed values between 0.5 and 2 mm for d, and 35–45° for θ, and found γ values between 2 and 20 as equivalent to 13–57% axial strain in our samples. An internal force gauge measured stress and an external LVDT mounted parallel to the specimen's shortening axis measured the axial strain. Water-saturated tests were performed under undrained conditions. Output signals were corrected for change in cross-sectional area of the specimens, friction, and distortion of loading column during deformation.

Experimental mechanical data is presented in Table 1. The transition from faulting to cataclastic flow (Rutter, 1986) occurred at 55–65 MPa in dry samples and at 80–100 MPa in the water-saturated samples. Stress-strain curves indicate strain-hardening cataclastic flow (Paterson, 1978) in samples deformed at pressures above 65 MPa, or taken to high strains at lower pressures. Cataclastic flow occurred on single and/or multiple fault zones depending on the level of strain. At high strains a set of curved conjugate shear zones were developed, creating a crush zone in the mid-section of barrel-shaped samples. The comminution process within the crush zones appears to involve shearing at large angles to σ_1 as well as compaction. A remarkable feature of the high-strain shear zones is the development of a cataclastic foliation clearly defined by displacement and shape change of iron oxide inclusions in the rock (Fig. 1).

Table 1
Mechanical data. F = shear fracture; SD = stress drop; CF = cataclastic flow; MF = multiple fault zone; H = strain-hardening; W = wet test

Sample	σ_3 (MPa)	% Axial strain	σ_{max} (MPa)	Mechanism
12	15	19.72	310.68	F, SD
1	35	18.78	312.48	F, SD
11	35	50.30	585.06	F, multiple SD, H
22w	55	13.00	286.56	F, multiple SD
20	55	53.20	506.88	CF, H
4	55	56.45	799.86	CF, H
5	55	57.00	738.50	CF, H
7	65	37.50	485.41	MF, H
9	65	49.00	714.47	MF, H
19	65	54.70	625.91	CF, H
10	85	50.00	728.85	CF, H
28w	100	12.97	293.42	F, multiple SD
38	100	14.35	472.21	CF, H
39	100	19.26	507.17	CF, H
40	100	24.00	539.74	CF, H
13	100	49.00	768.48	CF, H
41	100	28.00	584.62	CF, H
42	100	30.40	608.55	CF, H
45	100	34.00	611.23	CF, H
16	100	53.00	919.00	CF, H
30w	137	19.00	327.38	MF, H
31w	170	20.00	337.05	MF, H
47	200	14.16	643.40	CF, H
34	200	15.62	706.16	CF, H
54	200	26.50	740.60	CF, SD, H
53	200	26.70	691.78	CF, SD, H
36	200	51.03	998.12	CF, H

3. Analysis of the cataclastic textures

The range of PSDs for the deformed Massillon sandstone in Fig. 2 reveals that microstructural effects of cataclasis due to different axial strain are discernable only at $S \geq 7$ μm particle size. Below this particle size the distribution for all samples tend to merge (inset box in Fig. 2). Based on this observation we introduce comminution intensity, ψ, as a textural variable:

$$\psi = 1 - [A/(A_0 - \phi A_0)] \quad (1)$$

where A is the total sectional area of particle population ≥ critical size S_c in the PSD, A_0 is the total measurement area, and ϕ is the initial porosity. We note that the critical particle size value for the Massillon sandstone is about four times the suggested grinding limit of 1.7 μm for quartz (Kendall, 1978; Prasher, 1987). Our use of cumulative PSD in this analysis assumes that all experimental samples contain the finest size fractions. Microscopy (Fig. 3) supports the assumption that particle sizes in the order of the lower fractal limit (Sammis et al., 1987; Marone and Scholz, 1989; Blenkinsop, 1991) and quartz-grinding limit are produced at the lowest applied strain and pressure.

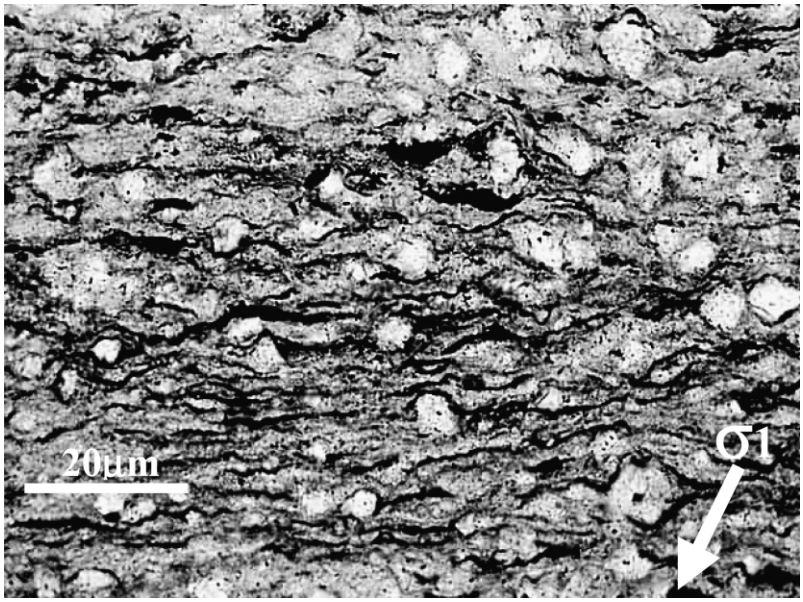

Fig. 1. Cataclastic foliation at high angles to σ_1 direction (arrow), typical of samples taken to high strains (sample 10 in Table 1). The microstructure is clearly defined by strings of sheared iron oxide inclusions. Optical PPL. Scale bar = 20 μm.

The data in Fig. 2 is consistent with the results of other studies of experimental and natural fault gouge that suggest a reduction in average particle size with strain (e.g. Sammis et al., 1987; Marone and Scholz, 1989; Sammis and Biegel, 1989; An and Sammis, 1994; Blenkinsop and Fernandez, 2000). It has been shown that with continued comminution the fracture probability for most particles diminishes as the average particle size approaches the grinding limit for the dominant mineral in the gouge (An and Sammis, 1994; Ozkan and Ortoleva, 2000). One possible explanation for particle size uniformity below S_c is that fragmentation comes to a halt in regions of the gouge where particle size has reached the mineral-grinding limit. It has been suggested that the finer particle size fractions might accommodate strain more by rolling (Morgan and Boettcher, 1999) and contact creep mechanisms than by comminution (Prasher, 1987; Opoczky and Farnady, 1984).

To further test the argument that comminution may not play a major role in deformation of particles less than 7 μm in our samples, we compared the D values for the full PSD of each sample with D values calculated based on the subset population of particles ≥7 μm. The fractal dimension values were derived from least square fit to log–log cumulative size–number plot of particles on three images from different parts of each sample at 100 × magnification (see data in Table 2 and next section for further details). A total of 2.2×10^5 particles from 80 images were measured. Over the range of applied strain the D values of the two sets, shown in Fig. 4, varied from each other only by 0–0.31 with a mean of 0.058, suggesting that the distribution of particle fraction less than 7 μm did not have a significant influence on D values. Similar results were reported for simulated gouge (Marone and Scholz, 1989) where D increased rapidly up to shear strains of about two, but leveled off at higher shear strains.

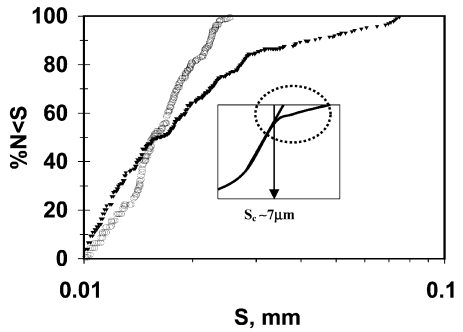

Fig. 2. Subset PSD plots for samples deformed at highest (circles: 57%), and lowest (triangles: 12.97%) axial strain. Data due to all other strain values fall within the range shown. Inset box is schematic drawing of the PSD down to ~3.5 μm particles. S_c is the critical particle size at the merger point of all PSD plots.

4. Textural measurements and results

Digital images (680 × 460) of the deformed Massillon sandstone were taken from polished thin sections at 100 × magnifications using reflected light optical microscopy. Use of the reflected-light imaging eliminated the 'noise' due to mineral composition. Images were taken with a computer-controlled digital still camera from areas inside fault zones in each deformed sample. Individual particle areas were measured automatically based on distinct pixel intensity of the particle surfaces against their background (Russ, 1999). Values for ψ were calculated based on measurements of approximately 6.1×10^5 particles from three different images of each of the 27 deformed samples. In each case

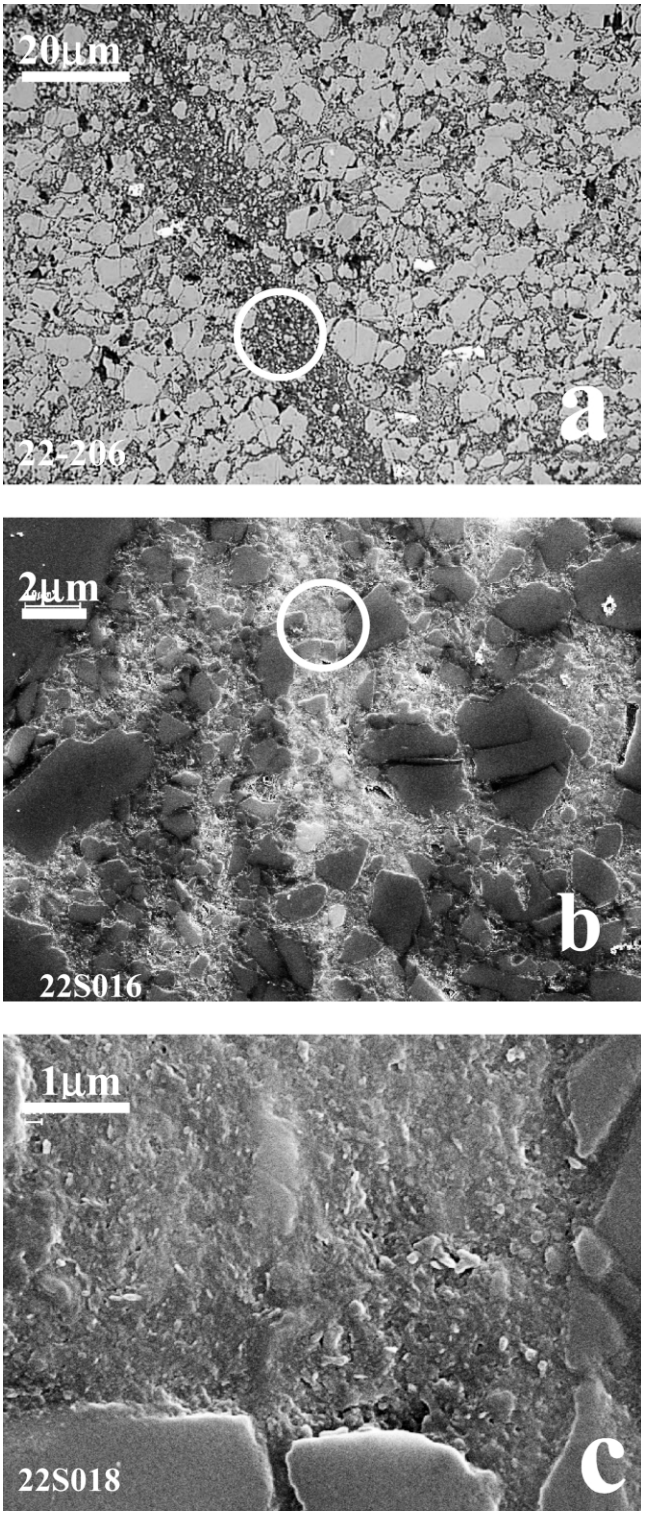

Fig. 3. Textures of deformed Massillon sandstone (sample 22, 35 MPa, and 13% strain). SEM close-ups of shear zone materials (circled areas) in (a) and (b) show the presence of extremely fine particles produced under conditions of low pressure and strain. Image (a) is optical reflected light.

the total area of particles ≥ 7 μm was used. A typical set of texture images with their corresponding comminution intensity values are shown in Fig. 5. The comminution intensity, and volume fractal dimension results are tabulated in Table 2, and their strain and pressure dependencies are shown in Fig. 6.

Table 2
Comminution intensity and volume fractal dimension of deformed Massillon sandstone microstructures. D, D_{min}, and D_{max} are values based on full PSD data. A subset of particles ≥ 7 μm was used to calculate 'D subset' values. All values are means of measurements made on three images from different parts of each sample

Sample	% ϵ	ψ	D_{min}	D_{max}	D	D subset
28w	12.97	0.5353	2.68	3.03	2.91	2.96
22w	13	0.5450	2.75	3.17	2.99	3.03
47	14.16	0.4780	2.72	2.96	2.87	2.90
38	14.35	0.5758	2.8	3.1	2.93	2.97
34	15.62	0.5415	2.74	3.13	2.95	3.00
1	18.78	0.5633	2.88	3.26	3.07	3.11
30w	19	0.5712	2.82	3.46	3.09	3.15
39	19.26	0.5356	2.73	3	2.85	2.90
12	19.72	0.6059	3.04	3.3	3.13	3.19
31w	20	0.6079	2.86	3.09	3.01	3.06
40	24	0.5852	2.93	2.97	2.94	2.99
54	26.5	0.5186	2.8	2.96	2.89	2.93
53	26.7	0.5380	2.85	2.89	2.86	2.92
41	28	0.6352	2.88	3.2	3.06	3.12
42	30.4	0.6872	2.79	2.89	2.85	2.95
45	34	0.6320	2.77	2.45	2.91	2.95
7	37.5	0.7574	3.13	3.41	3.3	3.33
9	49	0.8416	3.07	3.59	3.42	3.44
13	49	0.7719	2.96	3.37	3.21	3.24
10	50	0.7978	3.28	3.62	3.41	3.44
11	50.3	0.7623	3.08	3.35	3.19	3.24
36	51.03	0.8225	3.05	3.37	3.22	3.29
16	53	0.8539	3.31	3.69	3.51	3.51
20	53.2	0.8203	3.33	3.46	3.39	3.41
19	54.7	0.8034	3.32	3.66	3.44	3.46
4	56.45	0.7958	3.12	3.26	3.18	3.45
5	57	0.7844	2.98	3.19	3.05	3.26

The accuracy of particle area measurements for a given magnification is primarily dependent upon image resolution. Visual comparisons between the actual particle shape on the unprocessed image and shape of the overlay used for dimensional measurements show that the image processing software provided reliable area measurements for particles greater than 2-pixel

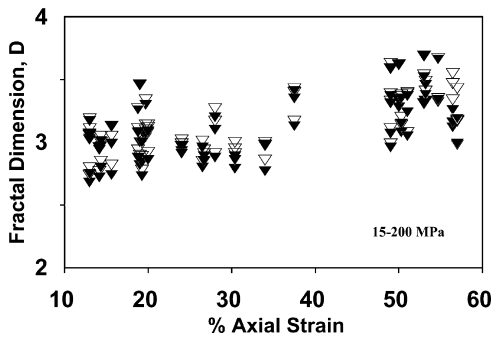

Fig. 4. Volume fractal dimension for Massillon sandstone samples deformed at various strain. Solid triangles are D values based on each sample's full PSD data, blank triangles are D values based on subset PSD (particles ≥ 7 μm) of the same samples.

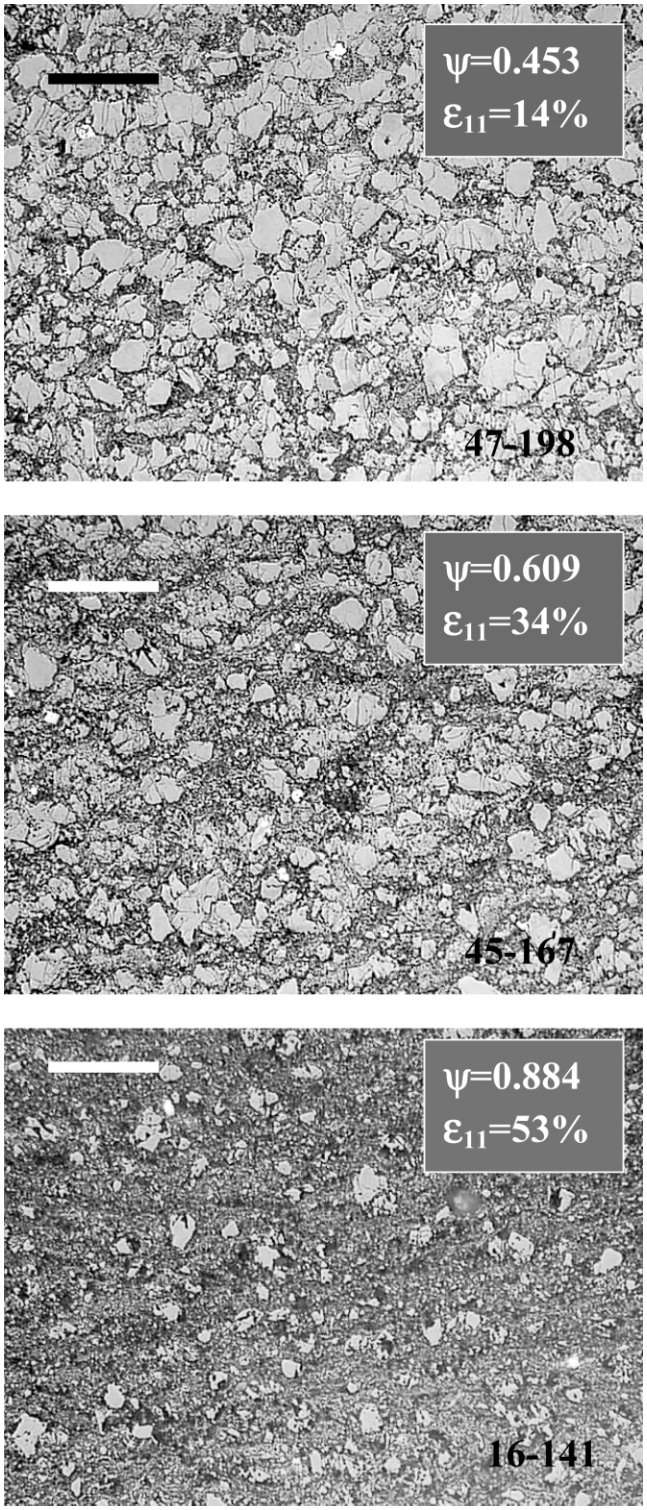

Fig. 5. Typical progression in comminution intensity with increased axial strain in three samples. The sample with the highest ψ value is foliated cataclasite similar to one shown in Fig. 1. Optical reflected light. Scale bar = 20 μm.

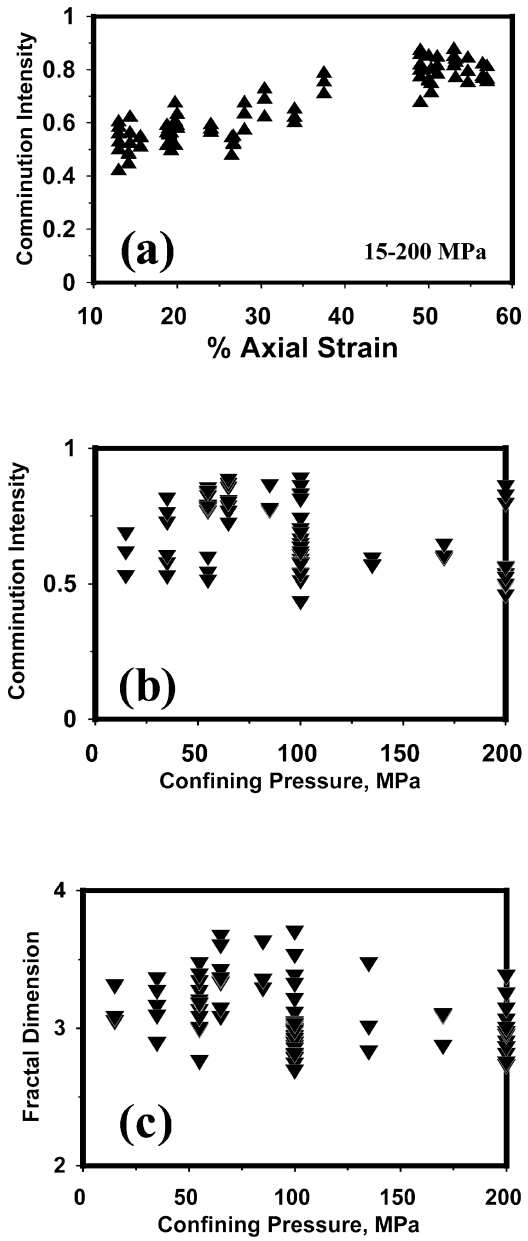

Fig. 6. (a)–(c). Strain and pressure dependence of the comminution intensity and volume fractal dimension for all deformed samples.

diameter, or $2 \times (1080\ \mu m/680) = 3.37\ \mu m$. Furthermore, in the case of comminution intensity values the use of particle size $\geq 7\ \mu m$ excluded fine particles such as alteration products, or phyllosilicates that might be difficult to image with reasonable accuracy.

5. Discussion

The data presented in Figs. 4 and 6 indicate that both comminution intensity, and fractal dimension directly correlate with the applied axial strain. Since there seems to be little or no correlation with pressure (Fig. 6b and c), only the relationship between strain, ψ, and D will be

discussed. Functional limits of the particle image area according to Eq. (1) are $(A_0 - \phi A_0) \geq A \geq 0$, requiring $1 \geq \psi \geq 0$, noting that based on the PSD analysis presented earlier we set $A = 0$ for $S_c < 7$ μm. The involvement of particles smaller than S_c in the comminution process is assumed to be negligible because of the approaching mineral grinding limit. If A is set to zero at the mineral-grinding limit (in this case ~ 1.7 μm), strain due to comminution will be overestimated at large strains. The S_c corresponding to $A = 0$ is probably mineral specific and should be determined via PSD measurements at different strains for major rock-forming minerals. We note that further studies will be necessary to investigate the relationship between this critical particle size range and the grain-scale deformation mechanisms in the brittle regime (e.g. fracture, rolling, contact creep).

Given the possible range of ψ values, the entire comminution intensity data plotted against axial strain (ϵ_{11}) fall within the bounds of curves of the power function $\psi = \epsilon_{11}^m$, with $0.25 \leq m \leq 0.5$ (Fig. 7a). The best fit to data is given by $m = 0.337$. The model functions extrapolating from the data predict that the rate of PSD evolution with respect to strain is initially very rapid, but diminishes above 20% strain. Since the data is based on microstructural measurements from areas of distributed cataclasis and does not factor in strain due to other mechanisms (e.g. localized slip) the model function would be only predictive of local strain, ϵ_L. Therefore, it may be suggested that where deformation is mainly accommodated via constrained comminution the strain might be predicted by:

$$\epsilon_L = \psi^n \tag{2}$$

where $n = 1/m$. Curves for n values two (upper bound) and four (lower bound) along with the best model for the Massilon microstructures, $\epsilon_L = \psi^{2.97}$, are shown in Fig. 7b. The greatest particle size variety, corresponding to the widest range of comminution intensities ($\psi \sim 0.14$ to 0.6), occurs at relatively low strains of about 2–13%.

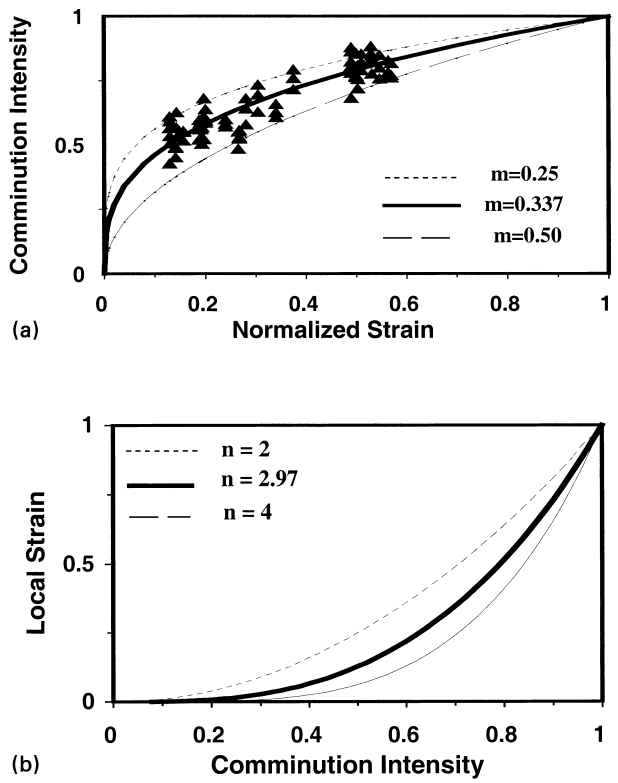

Fig. 7. Plots of the comminution intensity function. (a) Comminution intensity data fitted with curves of $\psi = \epsilon_{11}^m$ (b) Plots of the model function $\epsilon_L = \psi^n$.

It might appear that the fractal dimension data in Fig. 4 is as useful as the comminution intensity data in estimating a value for strain. However, we suggest that the method of estimating local strain via ψ^n has a number of advantages over the direct use of D values. While the S_c criterion ensures that ψ provides a measure of comminution, D values >2.6 are found to represent areas of fault gouge deformed by localized slip, or particle rolling (Allegre et al., 1982; Turcotte, 1986; Sammis et al., 1987; Marone and Scholz, 1989; Mair and Marone, 1999; Morgan and Boettcher, 1999). The comminution intensity relationship in Eq. (1) allows a certain degree of control in evaluation of particle surface area during image processing by inclusion, or exclusion of features such as cementation, transgranular factures, and SPO. Microstructurally interesting, but small areas of fault gouge containing a few large particles will provide measurable surface area while providing too few particles for calculating meaningful D values. Overall, ψ appears to be more sensitive to microstructural effects of the comminution process rather than the number of measured particles.

In general, the textural make-up of brittle fault zones consist of regions of different PSD, posed at various stages of evolution. The comminution intensity function could be used for millimeter to meter scale mapping of local strain in experimental samples and relative magnitude of comminution in natural fault gouge. The interpretation of such textural maps, simulated and/or real, would be helpful in understanding the micromechanical processes of the onset of shear localization, and changes in permeability structure in natural fault zones. It should be noted that the strain estimates would be useful only in quantifying strain due to the latest episode of brittle deformation, although this may not appear to be a serious concern in work with some experimental faults. Also, relationship (2) appears to be suitable for estimating strain in distributed cataclasis, and will probably underestimate strain if the sample image areas include significant slip surfaces. These limitations with texture-based strain measurements in cataclastic deformation have been noted previously (Sammis et al., 1987; An and Sammis, 1994; Gu and Wong, 1994).

6. Conclusions

The microstructural effects of experimental comminution at different axial strains in Massillon sandstone are discernible only at particle size $\geq 7\ \mu m$. The particle size distribution tends to merge for all samples below this particle size. While the textural developments appeared to be insensitive to changes in the applied confining pressure, fractal dimension increased steadily with increased axial strain. The observations suggest that locally, processes other than particle size reduction by fracture might become operative when a critical particle size is reached. Accordingly, local strain due to comminution may be estimated based on the textural parameters characteristics of particles greater than the critical size for the studied rock material.

Acknowledgements

The authors wish to thank Tom Blenkinsop, James P. Evans, and Karen Mair for their highly valuable comments. This research was in part supported by a grant to Hadizadeh from the Office of VP for Research at the University of Louisville.

References

Allegre, C.J., Le Mouel, J.L., Provost, A., 1982. Scaling rules in rock fracture and possible implications for earthquake prediction. Nature 297, 47–49.

An, L.-J., Sammis, C.G., 1994. Particle size distribution of cataclastic fault materials from southern California: a 3-D study. Pure and Applied Geophysics 143, 203–227.

Beeler, N.M., Tullis, T.E., Weeks, J.D., 1996. Frictional behavior of large displacement experimental faults. Journal of Geophysical Research 101, 8697–8715.

Biegel, R.L., Sammis, C.G., Dieterich, J.H., 1989. The frictional properties of a simulated gouge having fractal particle distribution. Journal of Structural Geology 11, 827–846.

Blenkinsop, T.G., 1991. Cataclasis and the processes of particle size reduction. Pure and Applied Geophysics 136, 59–86.

Blenkinsop, T.G., Fernandez, T.R., 2000. Fractal characterization of particle size distributions in chromitites from the Great Dyke, Zimbabwe. Pure and Applied Geophysics 157, 505–521.

Dieterich, J.H., 1981. Constitutive properties of faults with simulated gouge. In: Mechanical Behavior of Crustal Rocks, The Handin Volume. American Geophysical Union Monograph 24, pp. 103–120.

Evans, J.P., Chester, F.M., 1995. Fluid-rock interaction in faults of the San Andreas system: inferences from San Gabriel fault rock geochemistry and microstructures. Journal of Geophysical Research 100, 13007–13020.

Evans, J.P., Forester, C.B., Goddard, J.V., 1997. Permeability of fault-related rocks, implications for hydraulic structure of fault zones. Journal of Structural Geology 19, 1393–1404.

Gu, Y., Wong, T.-F., 1994. Development of shear zone localization in simulated quartz gouge; effect of cumulative slip and gouge particle size. Pure and Applied Geophysics 143, 387–423.

Kendall, K., 1978. The impossibility of comminuting small particles by compression. Nature 272, 710–711.

Lin, A., 2001. S–C fabric developed in cataclastic rocks from Nojima fault zone, Japan and their implications for tectonic history. Journal of Structural Geology 23, 1167–1178.

Logan, J.M., Rauenzahn, K.A., 1987. Frictional dependence of gouge mixtures of quartz and montmorillonite on velocity, composition and fabric. Tectonophysics 144, 87–108.

Mair, K., Marone, C., 1999. Friction of simulated fault gouge for a wide range of velocities and normal stresses. Journal of Geophysical Research 104, 28899–28914.

Mair, K., Main, I., Elphick, S., 2000. Sequential growth of deformation bands in the laboratory. Journal of Structural Geology 22, 25–42.

Marone, C., Scholz, C.H., 1989. Particle-size distribution and microstructures within simulated fault gouge. Journal of Structural Geology 11, 799–814.

Morgan, J.K., Boettcher, M.S., 1999. Numerical simulations of granular shear zones using the distinct element method 1. Shear zone kinematics and the micromechanics of localization. Journal of Geophysical Research 104, 2703–2719.

Opoczky, L., Farnady, R., 1984. Fine grinding and states of equilibrium. Powder Technology 39, 107–115.

Ozkan, G., Ortoleva, P.J., 2000. Evolution of the gouge particle size distribution: a Markov model. Pure and Applied Geophysics 157, 449–468.

Paterson, M.S., 1978. Experimental Rock Deformation—The Brittle Field, Minerals and Rocks Series Volume 13, Springer-Verlag, New York, 254pp.

Prasher, C.L., 1987. Crushing and Grinding Handbook, John Wiley and Sons, New York.

Rawling, J.C., Goodwin, L.B., Wison, J.L., 2001. Internal architecture, permeability structure, and hydrologic significance of contrasting fault-zone types. Geology 29, 43–46.

Russ, J.C., 1999. The Image-processing Handbook, 3rd ed, CRC Press/IEEE Press, 771pp.

Rutter, E.H., 1986. On the nomenclature of mode of failure transition in rocks. Tectonophysics 122, 381–387.

Sammis, C.G., Biegel, R.L., 1989. Fractals, fault-gouge, and friction. Pure and Applied Geophysics 131, 255–271.

Sammis, C.G., Osborne, R.H., Anderson, J.L., Mavowe, E., White, P., 1986. Self-similar cataclasis in the formation of fault gouge. Pure and Applied Geophysics 124, 53–77.

Sammis, C.G., King, G., Biegel, R., 1987. The kinematics of gouge deformation. Pure and Applied Geophysics 125, 777–812.

Scholz, C.H., Anders, M.H., 1994. The permeability of faults. In: Hickman, S., Sibson, R., Bruhn, R. (Eds.), Proceedings Workshop LXIII. The Mechanical Involvement of Fluids in Faulting. United States Geological Survey Open File Report #94-228, pp. 247–253.

Sibson, R.H., 1977. Fault rocks and fault mechanics. Journal of Geological Society of London 133, 191–213.

Turcotte, D.L., 1986. Fractals and fragmentation. Journal of Geophysical Research 91, 1921–1926.

Zhang, S., Tullis, T.E., Scruggs, V.J., 1999. Permeability anisotropy and pressure dependency of permeability in experimentally sheared gouge materials. Journal of Structural Geology 21, 795–806.